Chemical Physics Letters 610–611 (2014) 115–120

Contents lists available at ScienceDirect

Chemical Physics Letters

journal homepage: www.elsevier.com/locate/cplett

Microwave-assisted synthesis of spherical β-$Ni(OH)_2$ superstructures for electrochemical capacitors with excellent cycling stability

Anjon Kumar Mondal [a,*], Dawei Su [a,b], Shuangqiang Chen [a], Jinqiang Zhang [a], Alison Ung [a], Guoxiu Wang [a,*]

[a] Centre for Clean Energy Technology, School of Chemistry and Forensic Science, University of Technology, Sydney, Broadway, Sydney, NSW 2007, Australia
[b] Institute of Superconducting and Electronic Materials, University of Wollongong, Wollongong, NSW 2522, Australia

ARTICLE INFO

Article history:
Received 31 May 2014
In final form 10 July 2014
Available online 17 July 2014

ABSTRACT

A novel single-step microwave-assisted process has been developed to synthesize spherical β-$Ni(OH)_2$ superstructures without using any templates. Structure characterizations show that the spherical β-$Ni(OH)_2$ composed of twisted nanosheets was obtained. The electrochemical properties of the as-prepared materials were evaluated by cyclic voltammetry and chronopotentiometry technology in 2 M KOH solution. Due to the unique morphology, the prepared β-$Ni(OH)_2$ electrode displays a high specific capacitance of 2147 F g^{-1} at a discharge current of 1 A g^{-1} and outstanding cycling stability (99.5% capacitance retained after 2000 cycles), suggesting its potential application as an efficient electrode material for high-performance electrochemical capacitors.

1. Introduction

It is now emergent demand for advanced electrochemical energy storage systems in parallel with the development of energy production from renewable and green energy sources. Among the different energy storage systems electrochemical capacitors (ECs) and batteries are two most investigated technological systems which lead the state-of-the-art electrochemical energy storage systems [1–3]. Batteries can store large amount of energy in a lightweight compact structure and supply suitable power levels for many application, virtually all mobile electronic devices store energy chemically in them. However, slow charge–discharge rates and short cycle life of current battery technologies limits high-power applications. Electrochemical capacitors (ECs) also known as supercapacitors offer transient but extremely high power for hybrid electric vehicles and mobile electrical systems. It has been considered as one of the most promising energy storage systems because of the higher power densities, faster recharge capabilities and longer cycle lives over batteries and it has the capability to store more energy than conventional capacitors [4–6]. In general, ECs store energy either between the electrode and electrolyte interfaces as electrical double layer capacitors (EDLCs) or fast and reversible redox reaction between electroactive species in electrolytes and electrodes as pseudocapacitors [7,8]. The practical applications of supercapacitors are mostly hampered owing to the lack of low cost high-performance electrode materials. For instance, the specific capacitance of traditional EDLCs (carbon-based materials) is usually less than 200 F g^{-1}, which cannot meet the constantly growing demand for peak-power support of electric vehicles and so on [5,9]. On the other hand, the pseudocapacitors (metal oxides, hydroxides and conducting polymers) offer very high specific capacitance associated with reversible Faradic reactions occurring at the electrode surface and thus the energy density is several times greater than that of EDLCs [10–12].

To develop high-performance energy storage devices, one of the most advantageous approaches is the specific design of materials with advanced functions. Advancement in supercapacitor technology has mostly benefited from nanoscience. Significant research efforts have focused in the design and fabrication of nanostructured electrode materials for high performance energy storage devices due to the fast-rising demand for high-power applications such as electric vehicles and hybrid electric vehicles. The nanoscale structures create high surface area, which notably enhances the efficiency in utilizing the electrode material and thus improve the performance of electrode [13]. The development of nanostructured materials, especially metal oxides and hydroxides are pseudocapacitive materials, which have multiple valence states that are capable of rich redox reactions. Various type of metal oxides and hydroxides, such as RuO_2 [14], NiO [15,16] Co_3O_4 [17], MnO_2 [18,19] and $Ni(OH)_2$ [20,21] and their mixed oxides [22–24] are the

* Corresponding authors.
E-mail addresses: anjonmondal@yahoo.com, Anjon.K.Mondal@student.uts.edu.au (A.K. Mondal), Guoxiu.wang@uts.edu.au (G. Wang).

http://dx.doi.org/10.1016/j.cplett.2014.07.025
0009-2614/

most promising candidates for pseudocapacitor electrode materials. Among these materials $Ni(OH)_2$ is of particular interest due to its high specific capacitance, low cost and well-defined electrochemical redox activity [25–27]. Huang et al. fabricated nickel hydroxide electrodes with open ended hexagonal nanotube arrays and achieved high specific capacitance of 1328 $F g^{-1}$ at the current density of 1 $A g^{-1}$ [20]. Mesoporous nickel hydroxide with a maximum capacitance of 1718 $F g^{-1}$ has been reported by Xing et al. [28]. Ma et al. have described uniform $Ni(OH)_2$ nanostructures by using hydrothermal method. Among them, the flower-like $Ni(OH)_2$ nanostructures assembled from ultrathin nanoflakes show the maximum specific capacitance of 1715 $F g^{-1}$ at a scan rate of 5 $mV s^{-1}$ [21]. Owing to its excellent electrochemical properties, it has extensive applications in alkaline rechargeable nickel-based batteries [29–32]. Different methods have been reported for the preparation of nanostructured β-$Ni(OH)_2$, such as hydrothermal [33,34], solvothermal [35,36], electrodeposition [26], chemical precipitation [37,38] and sonochemical [39] methods. Recently, microwave method has also gained tremendous attention due to its homogeneous thermal transmission and short heating time [40,41]. Over the past few years, nano/micro superstructures constructed by nanometer-sized building blocks have been established to be one of the best materials for ECs. These hierarchical structures should take over the exclusive benefits of their main building blocks and acquire extra advantages from their superior secondary building blocks. These subunits should provide superstructures with fascinating properties such as increased surface area, easing mechanical stress, assisting the diffusion of foreign substances throughout the bulk material and so on [42,43]. In the charge storage mechanism, surface properties play significant role therefore, an active material with superior surface properties and high capacitive performance is indispensable for the development of advanced supercapacitor device [44,45].

In this letter, we reported the synthesis of uniform micro-sized spherical β-$Ni(OH)_2$, which is consisted of 2D nanosheets through a single step template free microwave method and investigated as electrochemical pseudo-capacitive materials for potential energy storage applications.

2. Experimental

2.1. Preparation of spherical β-$Ni(OH)_2$

In a typical preparation process of the spherical β-$Ni(OH)_2$, 0.2 g of $Ni(NO_3)_2{\cdot}6H_2O$ was dissolved by adding deionized (DI) water (30 mL). The solution was stirred at room temperature, following the addition of 0.275 g of glycine and 0.275 g of Na_2SO_4 salt. Then 1.5 mL of NaOH solution (5 M) was added dropwise under magnetic stirring to form a clear blue solution. The solution was heated in a microwave synthesizer (Model: NOVA-II) at 180 °C for 30 min and then cooled down to room temperature. The products were collected by filtration, washed with DI water and absolute ethanol for several times and finally dried in an oven at 60 °C for 6 h.

2.2. Materials characterization

The crystallographic information and morphologies of the prepared spherical $Ni(OH)_2$ were investigated using GBC MMA X-ray diffractometer (λ = 0.15405 nm), a field emission scanning electron microscopy (FESEM, Zeiss Supra 55VP) and transmission electron microscopy (TEM, JEOL 2011 TEM facility). Thermogravimetric analysis (TGA) was carried out by using the 2960 SDT thermal analyser with a temperature ramp of 10 °C min^{-1} from room temperature to 700 °C under an air atmosphere. The measurements and analysis of the specific surface area and porosity were performed through Brunauer–Emmett–Teller (BET) nitrogen adsorption–desorption isotherms and Barret–Joyner–Halenda (BJH) method, respectively by using a Micromeritics 3 Flex™ surface characterization analyzer at 77 K. Fourier transform infrared (FTIR) spectra were recorded on a Bruker Tensor 27 IR spectrometer using KBr as dispersant between 400 and 4000 cm^{-1}.

2.3. Electrochemical measurements

Electrochemical properties of the as-obtained spherical β-$Ni(OH)_2$ were conducted using a CHI 660C electrochemistry workstation using cyclic voltammetry and chronopotentiometry technology in a three electrodes cell, where the as-prepared spherical $Ni(OH)_2$ was used as the working electrode, Pt foil as the counter electrode and saturated calomel electrode (SCE) as the reference electrode in 2 M KOH solution. The working electrodes were prepared by mixing the as-prepared material as active material, acetylene black as conducting material and polyvinylidene fluoride (PVDF) binder with a weight ratio of 70:20:10. A small amount of N-methyl-2-pyrrolidinone was added to the mixture to form slurry. The slurry was coated (area of coating: 1 cm^2, and a total mass of around 1 mg) onto pre-treated nickel foam for electrical conductivity and dried under vacuum at 100 °C for 12 h. The specific capacitance was calculated from both cyclic voltammetry (CV) and galvanostatic charge–discharge measurements.

3. Results and discussion

The crystal structure and purity of the as-prepared spherical $Ni(OH)_2$ was examined by X-ray diffraction (XRD) as shown in Figure 1. All diffraction peaks in Figure 1 can be indexed perfectly to a hexagonal crystal phase of β-$Ni(OH)_2$ (JCPDS card No. 14-0117). No peaks of any other phases or impurities are detected, suggesting the high purity of the as-synthesized β-$Ni(OH)_2$.

The morphology of the as-prepared spherical β-$Ni(OH)_2$ was examined by FESEM. Figure 2(a) and (b) shows the low magnification SEM images of the as-prepared sample, which indicating the formation of uniform numerous micro-sized spherical structures of β-$Ni(OH)_2$ with sizes around 2.0 μm. These micro-sized spheres have a 3D hierarchical urchin-like nanostructure, which is constructed from 2D nanosheets interconnected with each other and have interior cavities as shown in the high magnification SEM images (Figure 2(c) and (d)).

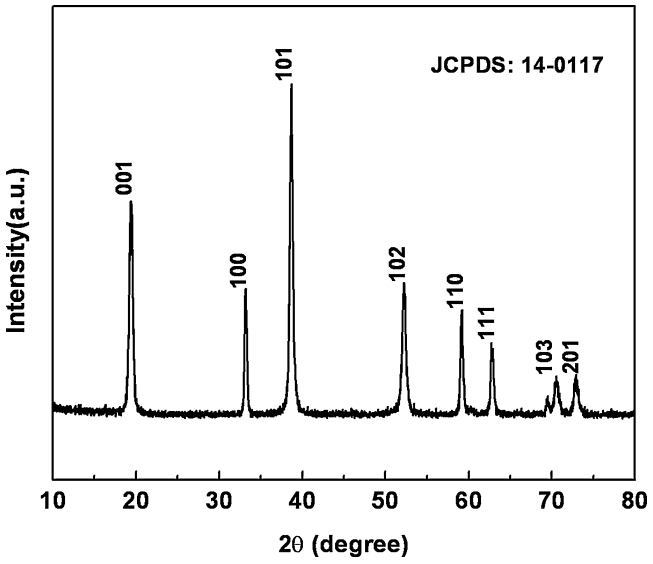

Figure 1. XRD pattern of spherical β-$Ni(OH)_2$.

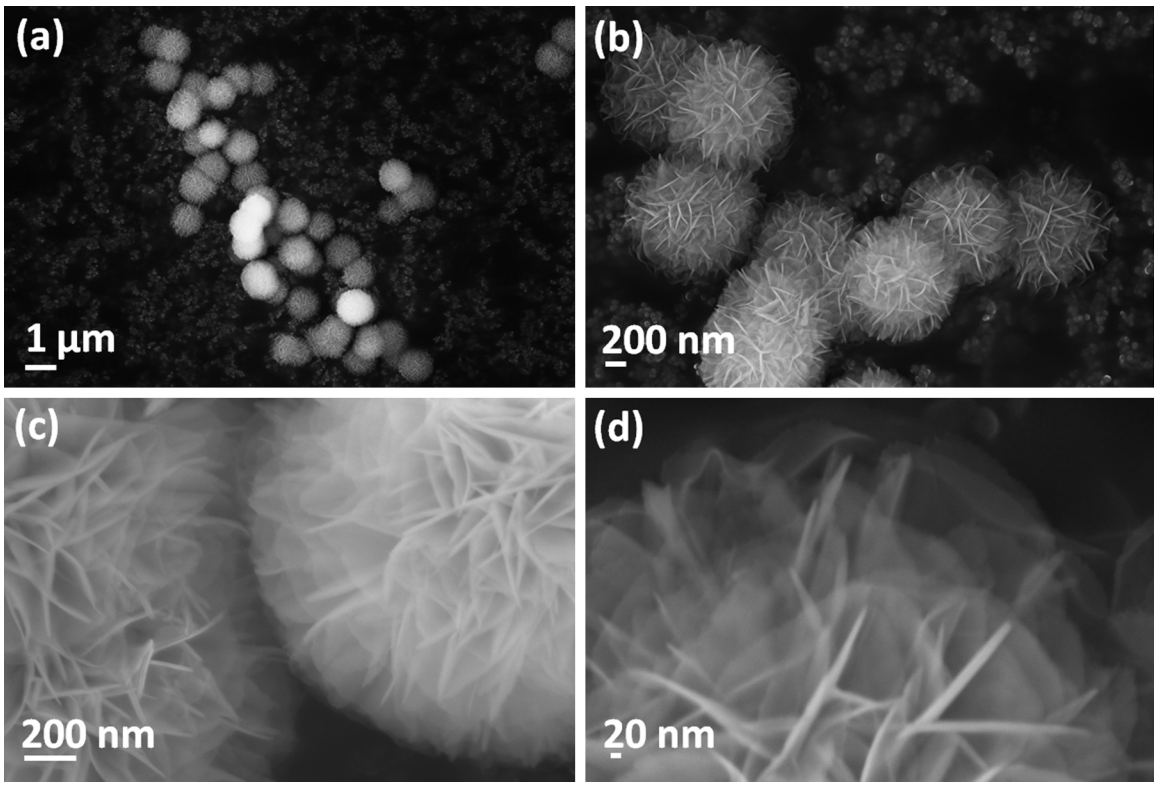

Figure 2. FESEM images of spherical β-$Ni(OH)_2$ (a and b) low magnification, (c and d) high magnification.

We further used transmission electron microscopy (TEM) and selected-area electron diffraction (SAED) patterns to identify the microstructure of as-prepared spherical β-$Ni(OH)_2$ as shown in Figure 3. It can be clear seen that in general the product is mainly micro-sized spherical shape with the uniform particle size from the low magnification TEM image (Figure 3(a)). All the selected area electron diffraction (SAED) patterns rings (Figure 3(b)) taken from the corresponding single spherical $Ni(OH)_2$ can be readily

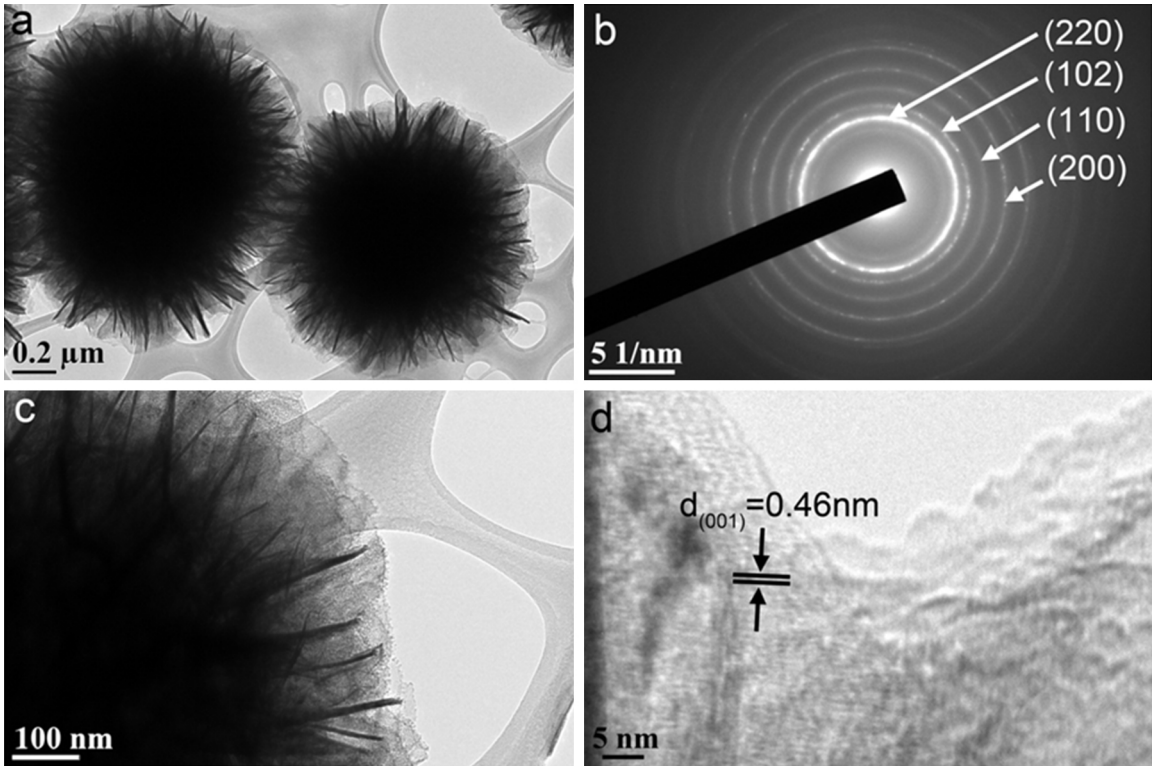

Figure 3. (a) Low magnification TEM image of spherical β-$Ni(OH)_2$ (b) is its corresponding selected area electron diffraction patterns (SAED), (c) high magnification TEM image and (d) lattice resolved HRTEM image.

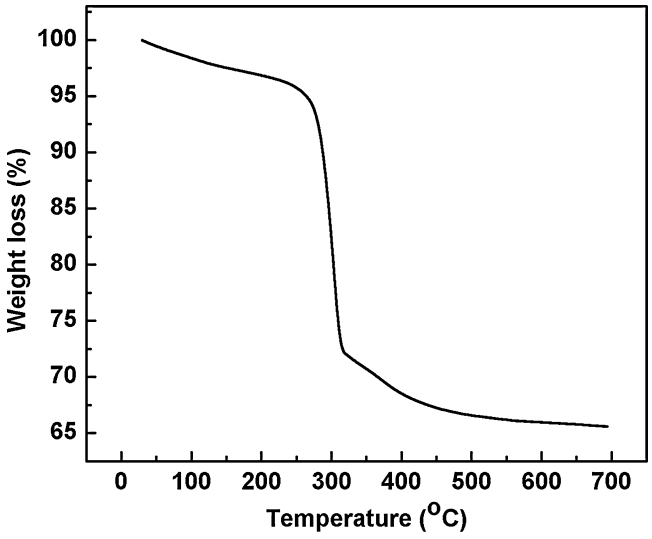

Figure 4. TGA curve of as-synthesized spherical β-Ni(OH)$_2$.

indexed to the hexagonal Ni(OH)$_2$ crystal structure. The high magnification TEM image (Figure 3(c)) illustrated the spherical Ni(OH)$_2$ were consisted of nanosheets. Figure 3(d) shows the lattice resolved HRTEM image of the Ni(OH)$_2$ nanocrystal, in which the (0 0 1) crystal plane with 0.46 nm d spacing can be observed directly, further confirming the crystal structure of the as-prepared Ni(OH)$_2$.

Thermogravimetric analysis (TGA) of the as-synthesized spherical β-Ni(OH)$_2$ was carried out between room temperature and 700 °C, as shown in Figure 4. The first 5.3% weight loss before 260 °C can be ascribed to the loss of absorbed water. The rapid weight loss from 260 °C to 322 °C is assigned to the decomposition of Ni(OH)$_2$ to NiO. It is noted that at the temperature range between 500 °C and 700 °C there is no obvious weight loss observed, which indicates the complete decomposition of Ni(OH)$_2$, the absence of any other phases and structural integrity.

Figure 5 shows the FTIR spectrum, which reveals chemical information and major functional groups of the as-prepared spherical β-Ni(OH)$_2$. A narrow and sharp peak at 3640 cm^{-1} is related to the υ(OH) stretching vibration of non-hydrogen bonded hydroxyl groups, which confirms the brucite structure of β-Ni(OH)$_2$ phase. The broad band at 3444 cm^{-1} is assigned to the O—H

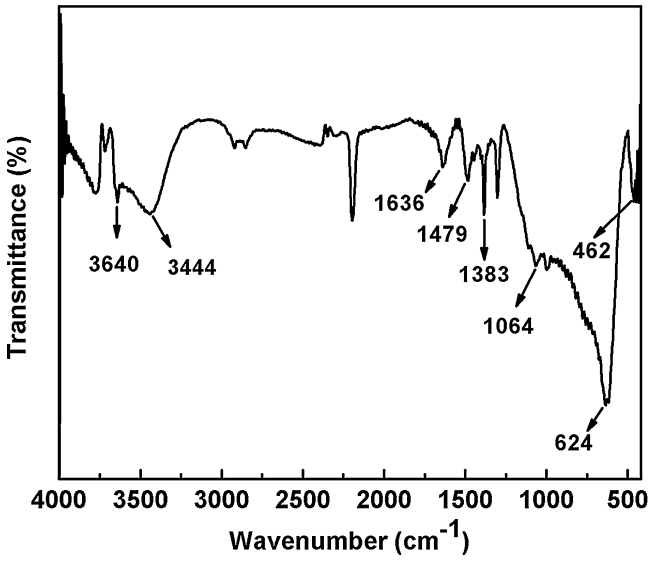

Figure 5. FTIR spectrum of the prepared spherical β-Ni(OH)$_2$.

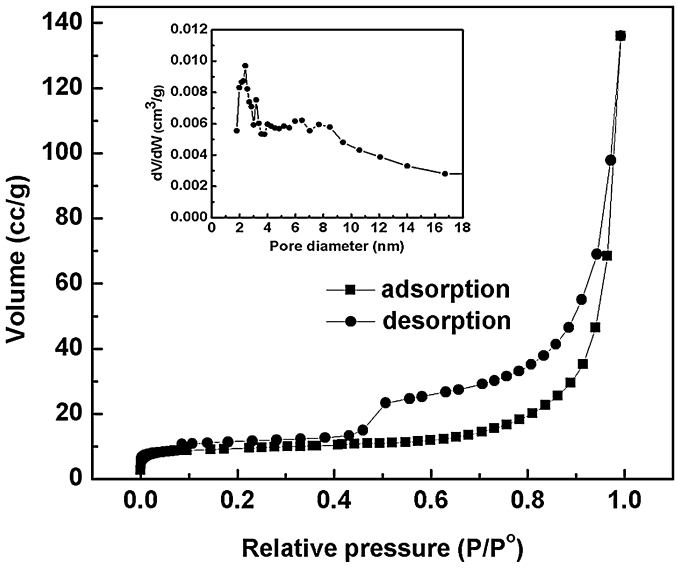

Figure 6. Nitrogen adsorption and desorption isotherm and pore size distribution curve of spherical β-Ni(OH)$_2$.

stretching vibration of interlayer water molecules and hydrogen bound hydroxyl groups. A strong absorption at 1636 cm^{-1} can also be attributed to the stretching and bending modes of surface-adsorbed water molecules [46]. The peak at 624 cm^{-1} is ascribed to the hydroxyl group lattice vibration δ(OH) and the absorption 462 cm^{-1} corresponding to the stretching vibration of Ni—OH (υ_{Ni-OH}) [46]. The peak at 1383 cm^{-1} could be attributed to a trace surface adsorption of nitrate (NO_3^-) ions originating from the starting nickel nitrate. Due to the basicity of metal hydroxides, it is normal to adsorb atmospheric carbon dioxide and the peaks observed at 1636 cm^{-1}, 1479 cm^{-1} and 1064 cm^{-1} are assigned to the presence of carbonate anions on the surface of spherical β-Ni(OH)$_2$ [37].

The specific surface area and porous nature of the as-prepared spherical β-Ni(OH)$_2$ were studied by N_2 adsorption and desorption measurements, as presented in Figure 6. From Figure 6 we can observe that the curve can be classified as typical Langmuir type IV isotherms with an obvious hysteresis loop, indicating that the material has mesoporous structure [47]. The mesoporous structure was further supported by the BJH pore size distribution data shown in the inset of Figure 6. The pore size distribution exposes with a mean pore diameter of 2.4 nm. The BET surface area of the spherical β-Ni(OH)$_2$ are calculated to be around 76 m^2 g^{-1}. Such large surface area and mesoporous structure can facilitate the transfer of ions and electrons at the electrode/electrolyte interface and are considered to be very suitable for application in supercapacitors.

The electrochemical properties of spherical β-Ni(OH)$_2$ as electrode material for supercapacitors were investigated. To evaluate the electrochemical properties cyclic voltammetry (CV) and chronopotentiometry measurements were carried out in a three-electrode cell. Figure 7(a) gives the galvanostatic charge–discharge profiles in an aqueous 2 M KOH electrolyte between 0 and 0.4 V (*vs.* SCE) at different current densities ranging from 1 A g^{-1} to 10 A g^{-1}. The nonlinear shape of charge–discharge curves confirmed the pseudocapacitive behaviour of β-Ni(OH)$_2$. The specific capacitance can be calculated by the formula, $C = I\Delta t/m\Delta V$, in which I is the discharge current, Δt refers the discharge time, m denotes the mass of the active material and ΔV represents the voltage window. Hence, the calculated specific capacitances are 2147, 1775, 1437 and 975 F g^{-1} corresponding to discharge current densities of 1, 2, 5 and 10 A g^{-1}, respectively. Figure 7(b) shows the representative CV curves of spherical β-Ni(OH)$_2$ electrode tested in an aqueous 2 M

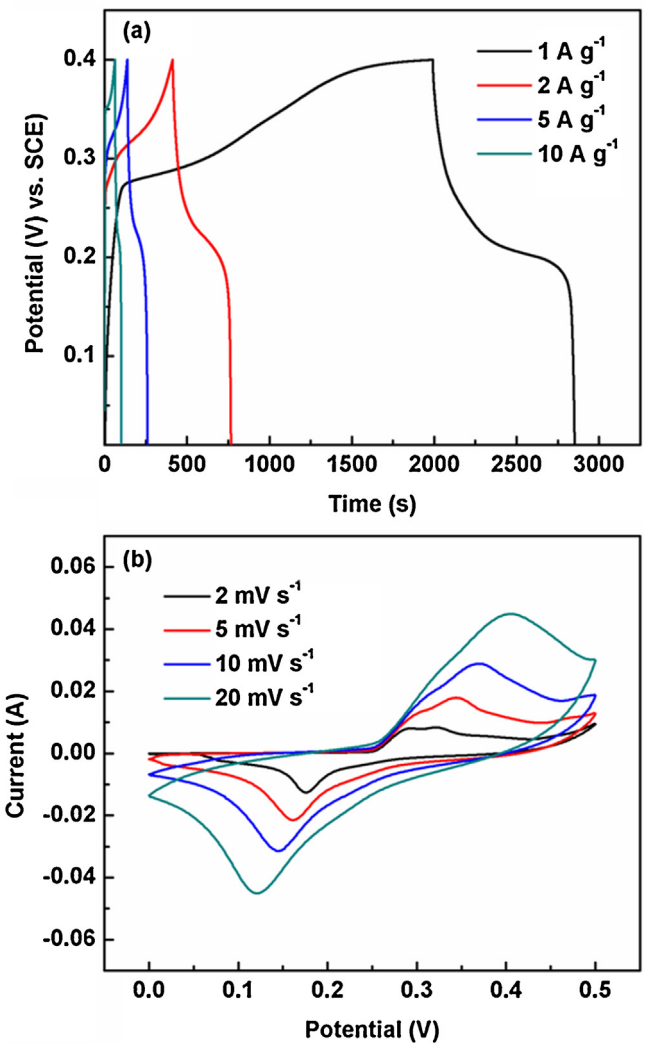

Figure 7. (a) Galvanostatic charge/discharge curves at different current densities (1–10 A g^{-1}) and (b) CV curves at various scan rates ranging from 2 to 50 mV s^{-1} for the spherical β-$Ni(OH)_2$ electrode in 2 M KOH electrolyte.

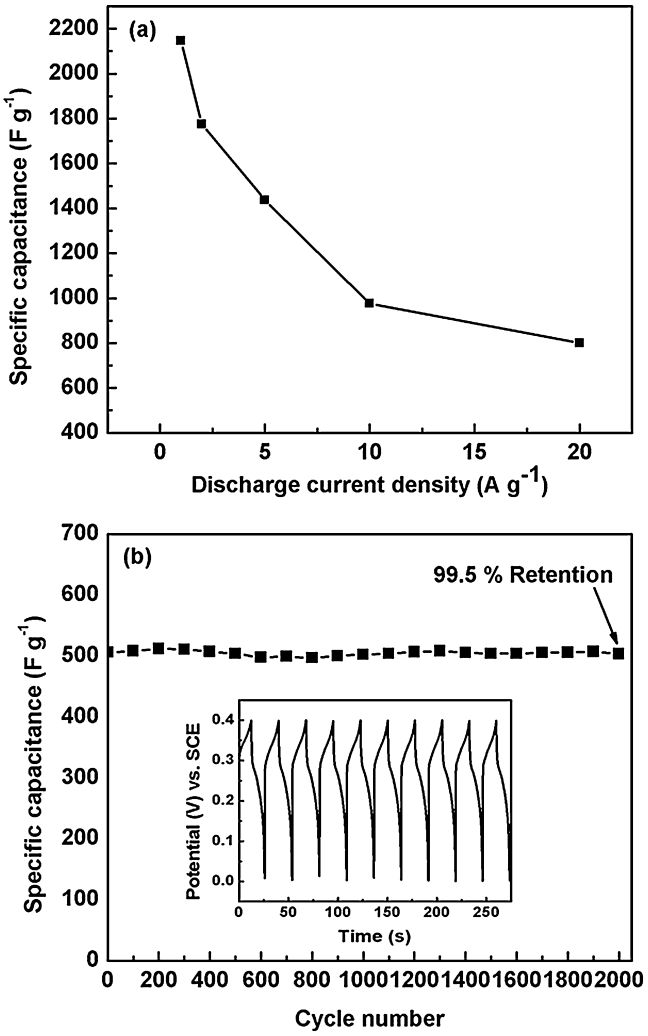

Figure 8. (a) Specific capacitance at various discharge current densities and (b) cycling performance of spherical β-$Ni(OH)_2$ at a scan rate of 50 mV s^{-1}. The charge and discharge curves of β-$Ni(OH)_2$ for the first ten cycles (the inset in Figure 8(b)).

KOH electrolyte at different scan rates within the potential window of 0–0.5 V (*vs.* SCE). In all CV curves, a pair of redox peaks is clearly observed and the shapes of the CV curves are well distinguished from that of the EDLC, which reveals the energy storage mechanism of β-$Ni(OH)_2$ primarily originates from faradic redox reactions. At the scan rate of 2 mV s^{-1} the anodic peak (positive current density) observed around 0.3 V (*vs.* SCE) indicates an oxidation of $Ni(OH)_2$ to NiOOH, whereas the cathodic peak (negative current density) detected around 0.17 V (*vs.* SCE) corresponds to the reverse process. It is well recognized that the surface Faradic reaction for $Ni(OH)_2$ electrode material will proceed according to the following reaction [48]:

$$Ni(OH)_2 + OH^- \leftrightarrow NiOOH + H_2O + e^- \quad (1)$$

When the scan rates increase from 2 to 20 mV s^{-1} the shape of the CV curves does not change significantly, which reveals excellent electrochemical reversibility of the electrode owing to the facile ion diffusion and good adsorption behaviour of β-$Ni(OH)_2$ electrode. The corresponding specific capacitance was also calculated from the CV curves according to the equation, $C = Q/\upsilon m \Delta V$, where Q is the charge obtained by integrating the CV curves, υ is the scan rate, m is the mass of active material and ΔV is the potential window of each scan. According to the CV curves the calculated values to be 1909, 1720, 1369 and 1051 F g^{-1} at the scan rate of 2, 5, 10, and 20 mV s^{-1}, respectively. The specific capacitance determined from both charge–discharge and CV curves is much higher than the previously reported β-$Ni(OH)_2$ nanoflakes [21], β-$Ni(OH)_2$ nanoparticles [26] and mesoporous nickel hydroxide [28]. The high specific capacitance can be attributed to the unique micro-sized spherical structure constructed by nanosheets which provides high specific surface area and effective diffusion channels. These diffusion channels reduce the diffusion length for the electrolyte ions, guarantees rapid contact of electrolyte ions to the large surfaces of electroactive β-$Ni(OH)_2$. The β-$Ni(OH)_2$ consist of nanosheets connected with each other and interior cavities, which act as 'ion-buffering reservoirs' and effectively mitigate the volume expansion during charge/discharge cycling. As a result, the unique spherical β-$Ni(OH)_2$ electrode can achieve a high electrochemical utilization even at high current densities and high scan rates.

Figure 8(a) shows the specific capacitances of spherical β-$Ni(OH)_2$ electrode at different current densities. When the current density increases from 1 A g^{-1} to 20 A g^{-1} the specific capacitances noted to decrease, which can be ascribed to the presence of inner active sites that are incapable to take part complete redox transitions at high current densities. This suggests that the parts of the electrode surfaces are unreachable at high current densities [49].

The long-term cycling performance is one of the most significant parameters for practical application of supercapacitors. The spherical β-Ni(OH)$_2$ was further tested by repeating CV tests over 2000 cycles at the scan rate of 50 mV s^{-1} as demonstrated in Figure 8(b). Notably, capacitance deterioration is only 0.5% after 2000 continuous cycles, indicating the excellent long-term cycling stability. It is also worth noting that the charge and discharge curves of spherical β-Ni(OH)$_2$ (inset in Figure 8(b)) for the first ten cycles are nearly same at the current density of 20 A g^{-1}, which also confirming the excellent electrochemical reversibility of the β-Ni(OH)$_2$ electrode. Thus, the spherical β-Ni(OH)$_2$ assembled from nanosheets demonstrate superior specific capacitance with excellent cycling stability, making them promising electrode materials for practical applications.

4. Conclusions

In summary, we propose a simple but efficient strategy to prepare uniform spherical β-Ni(OH)$_2$ superstructures, which is composed of nanosheets. Such a unique morphology with mesoporous character facilitates fast ion and electron transport, alleviates the volume expansion during OH^- insertion and extraction process and ensures adequate Faradic reactions at high current densities for energy storage. Electrochemical results show that the spherical β-Ni(OH)$_2$ demonstrates a high specific capacitance of 2147 F g^{-1} at 1 A g^{-1} and excellent cycling stability (0.5% capacitance loss after 2000 cycles). Importantly, this facile and cost-effective strategy could be extended to the preparation of other electroactive materials for electrochemical capacitors.

Acknowledgement

The authors are thankful for the financial support provided by the Australian Research Council (ARC) through the ARC discovery project (DP1093855).

References

[1] M. Winter, R.J. Brodd, Chem. Rev. 104 (2004) 4245.
[2] P. Simon, Y. Gogotsi, Nat. Mater. 7 (2008) 845.
[3] S. Arico, P. Bruce, B. Scrosati, J.M. Tarascon, S.W. Van, Nat. Mater. 4 (2005) 366.
[4] J.R. Miller, P. Simon, Science 32 (2008) 651.
[5] G.P. Wang, L. Zhang, J.J. Zhang, Chem. Soc. Rev. 41 (2012) 797.
[6] A. Burke, J. Power Sources 9 (2000) 37.
[7] E. Frackowiak, F. Beguin, Carbon 39 (2001) 937.
[8] B.E. Conway, J. Electrochem. Soc. 138 (1991) 1539.
[9] M. Kaempgen, C.K. Chan, J. Ma, Y. Cui, G. Gruner, Nano Lett. 9 (2009) 1872.
[10] B. Wang, J.S. Chen, Z.Y. Wang, S. Madhavi, X.W. Lou, Adv. Energy Mater. 2 (2012) 1188.
[11] R. Kotz, M. Carlen, Electrochim. Acta 45 (2000) 2483.
[12] T. Brezesinski, J. Wang, S.H. Tolbert, B. Dunn, Nat. Mater. 9 (2010) 146.
[13] Q. Lu, J.G. Chen, J.Q. Xiao, Angew. Chem. Int. Ed. 52 (2013) 1882.
[14] N. Kang, T. Yu, G.H. Lim, T. Koh, B. Lim, Chem. Phys. Lett. 592 (2014) 192.
[15] X. Xia, J. Tu, X. Wang, C. Gu, X. Zhao, J. Mater. Chem. 21 (2011) 671.
[16] S.K. Meher, P. Justin, G.R. Rao, ACS Appl. Mater. Interfaces 3 (2011) 2063.
[17] A.L.M. Barmi, M. Aghazadeh, B. Arhami, H.M. Shiri, A.A. Fazl, E. Jangju, Chem. Phys. Lett. 541 (2012) 65.
[18] S. Devaraj, N. Munichandraiah, J. Phys. Chem. C 112 (2008) 4406.
[19] M. Xu, L. Kong, W. Zhou, H. Li, J. Phys. Chem. C 111 (2007) 19141.
[20] M.S. Wu, K.C. Huang, Chem. Commun. 47 (2011) 12122.
[21] H. Jiang, T. Zhao, C. Li, J. Ma, J. Mater. Chem. 21 (2011) 3818.
[22] J. Yan, E. Khoo, A. Sumboja, P.S. Lee, ACS Nano 4 (2010) 4247.
[23] T.Y. Wei, C.H. Chen, H.C. Chien, S.Y. Lu, C.C. Hu, Adv. Mater. 22 (2010) 347.
[24] J. Liu, J. Jiang, C. Cheng, H. Li, J. Zhang, H. Gong, H.J. Fan, Adv. Mater. 23 (2011) 2076.
[25] G. Hu, C. Li, H. Gong, J. Power Sources 195 (2010) 6977.
[26] M. Aghazadeh, A.N. Golikand, M. Ghaemi, Int. J. Hydrogen Energy 36 (2011) 8674.
[27] G. Fu, et al., Int. J. Electrochem. Sci. 4 (2009) 1052.
[28] S. Xing, Q. Wang, Z. Ma, Y. Wu, Y. Gao, Mater. Lett. 78 (2012) 99.
[29] F.S. Cai, G.Y. Zhang, J. Chen, X.L. Gou, H.K. Liu, S.X. Dou, Angew. Chem. Int. Ed. 43 (2004) 4212.
[30] J. Chen, D.H. Bradhurst, S.X. Dou, H.K. Liu, J. Electrochem. Soc. 146 (1999) 3606.
[31] T.K. Ying, X.P. Gao, W.K. Hu, F. Wu, D. Noreus, Int. J. Hydrogen Energy 31 (2006) 525.
[32] E. Shangguan, Z. Chang, H. Tang, X.Z. Yuan, H. Wang, Int. J. Hydrogen Energy 35 (2010) 9716.
[33] L.X. Yang, Y.J. Zhu, H. Tong, Z.H. Liang, L. Li, L. Zhang, J. Solid State Chem. 180 (2007) 2095.
[34] L. Kumari, W.Z. Li, Physica E 41 (2009) 1289.
[35] B.N. Wang, X.Y. Chen, D.W. Zhang, J. Phys. Chem. Solids 71 (2010) 285.
[36] D. Yang, R. Wang, M. He, J. Zhang, Z. Liu, J. Phys. Chem. B 109 (2005) 7654.
[37] S. Zhang, H.C. Zeng, Chem. Mater. 21 (2009) 871.
[38] M. Cao, X. He, J. Chen, C. Hu, Cryst. Growth Des. 7 (2007) 170.
[39] M. Vidotti, C. Greco, E.A. Ponzio, S.C. Torresi, Electrochem. Commun. 8 (2006) 554.
[40] G.A. Tompsett, W.C. Conner, K.S. Yngvesson, Chem. Phys. Chem. 7 (2006) 296.
[41] I. Bilecka, M. Niederberger, Nanoscale 2 (2010) 1358.
[42] L.R. Hou, C.Z. Yuan, L. Yang, L.F. Shen, F. Zhang, X.G. Zhang, RSC Adv. 1 (2011) 1521.
[43] W. Wei, Z.Z. Yang, Adv. Mater. 20 (2008) 2965.
[44] F. Wang, S. Xiao, Y. Hou, C. Hu, L. Liu, Y. Wu, RSC Adv. 3 (2013) 13059.
[45] W. Deng, X. Ji, Q. Chen, C.E. Banks, RSC Adv. 1 (2011) 1171.
[46] P. Oliva, et al., J. Power Sources 8 (1982) 229.
[47] A. Vinu, D.P. Sawant, K. Ariga, M. Hartmann, S.B. Halligudi, Microporous Mesoporous Mater. 80 (2005) 195.
[48] J. Yan, W. Sun, T. Wei, Q. Zhang, Z. Fan, F. Wei, J. Mater. Chem. 22 (2012) 11494.
[49] U.M. Patil, K.V. Gourav, V.J. Fulari, C.D. Lokhande, O.S. Joo, J. Power Sources 188 (2009) 338.